SCIPEDIA Revista Internacional de Métodos Numéricos para Cálculo y Diseño en Ingeniería

Revista Internacional Métodos numéricos para cálculo y diseño en ingeniería RIMNI

Design and characteristic analysis of dual-excitation and dual-modulation axial permanent magnetic gear

Yanjun Ge[1], Fang Liu[1], Daming Wang[1], Dongning Liu[1]

1 School of Mechanical Engineering, Dalian Jiaotong University, Dalian, China

Abstract

Due to marked axial and tangential magnetic leakage and low torque density of APMG, an external magnetic regulating ring is developed in this study based on APMG to form a DEM-APMG structure of bidirectional excitation and bidirectional modulation. The low-speed permanent magnet rotor of the DEM-APMG is sandwiched between the inner and outer flux regulating rings, which can convert the axial and tangential flux leakage of the APMG into useful harmonics to increase the output torque and torque density of the DEM-APMG. In this study, mathematical analysis is used to describe the air gap magnetic density and electromagnetic torque model of a DEM-APMG, which essentially describes the root cause of the increase in torque density. Using 3-D finite element static and dynamic simulations, the transmission characteristics of the APMG and DEM-APMG are compared and analyzed. Results show that the maximum static torque of the DEM-APMG high-speed and low-speed permanent magnet rotor with the same outer diameter increase by 22.7% and 23.8%, respectively, compared with APMG, 26% and 29%, respectively, in steady-state operation, and the torque density increases by 24%. The influence of the primary structural parameters on the transmission characteristics is also investigated using the control variable method. Results show that the duty cycle of the magnet adjusting block, the axial length of the high-speed permanent magnet and the low-speed permanent magnet have the strongest effect on the torque density of the DEM-APMG. When the axial length of the high-speed permanent magnet and low-speed permanent magnet is 8mm, and the duty cycle is 0.4, the torque density can reach the optimal value of 156kNm/m^3.

OPEN ACCESS

Published: 02/12/2022

Accepted: 29/11/2022

DOI:
10.23967/j.rimni.2022.12.001

Keywords:
Air gap magnetic tightness
Torque density
Axial excitation
Axial modulation
Axial Permanent Magnet Gear

1. Introduction

Permanent magnet gears (PMG) transmit speed and torque through mutual coupling of magnetic fields, which has the advantages of high utilization rate of permanent magnet, large electromagnetic torque and automatic overload protection. PMG can be divided into magnetic radial and axial according to the magnetic circuit structure. A radial permanent magnet gear (RPMG) was thus proposed [1], and a two-dimensional gas gap magnetic field and torque model and a torque density of 100kNm/m^3 were calculated using the finite element method. Because RPMG is a three-layer rotor, a two-layer air gap, and the complex structure of the magnetic regulation ring, experimental prototype manufacturing is difficult. Thus, Axial Permanent Magnet Gear (APMG) was proposed based on RPMG, which does not require accurate alignment, its magnetic tuning ring is simpler than RPMG, the axial distance is small, and the prototype is easy to manufacture and easy to apply in production practice [2].

The primary disadvantage of APMG is that the axial and tangential partial magnetic roads are not closed, and there is a relatively serious magnetic leakage, resulting in a low torque density (generally 70kNm/m^3). In this paper, a double-excitation modulation APMG structure (DEM-APMG) is proposed.

The DEM-APMG adds a magnetization ring (external magnetization ring) to the APMG so that the low-speed permanent magnet on the low-speed rotor can produce a two-way excitation magnetic field and be modulated by two magnetization rings to transfer the torque. Due to the external magnetic loop, the low-speed rotor can be modulated by the internal and external magnetic modulation loop concurrently, transforming the leakage magnetic flux in the APMG air gap into useful harmonics and acting again on the low-speed rotor, effectively improving the utilization rate of the low-speed permanent magnet and increasing the torque transfer ability. After 3D finite element simulation, the torque density of the DEM-APMG is found to be approximately 150kNm/m³.

Because a 2D finite element analysis cannot describe the ends of axial and tangential magnetic paths in this configuration, the effect of the magnetic path structure on the torque density cannot be accurately evaluated [3]. Thus,

Correspondence: Daming Wang (wangdaming1987@163.com).

a 3D finite element model that does describe the end effects of the APMG magnetic field was developed [4], and the air-gap magnetic density distribution of the APMG and its torque properties were obtained.

To verify the feasibility of the 3D finite-element analysis, the APMG experimental prototype was made using 3D printing technology and performed with 3D finite element simulation and static and dynamic experiments [5]. Results show that the 3D finite element simulation and the experimental test agreed with a static and dynamic error of approximately 4.5%, indicating that the 3D finite element simulation is accurate and reliable.

In addition, the modulation mechanism of APMG was analyzed by establishing a 3D mathematical model, and the calculation results are basically consistent with the experimental test [6]. Compared to the 3D finite element simulation, the 3D mathematical model is comparable to its computational accuracy but is faster and easier to analyze and optimize its structural parameters [7].

Based on the operating mechanism of APMG, we establish a dual-excitation and dual-modulation DEM-APMG mechanical model and 3D mathematical model to describe the fundamental cause of DEM-APMG torque density and analyze the transmission characteristics of APMG and DEM-APMG.

2. Analysis of the DEM-APMG

Figure 1 shows the existing mechanical structure of the APMG, whose working principle is as follows: when the number of APMG magnetic modulation blocks is equal to the sum of the magnetic log of the high-speed rotor and the low-speed rotor pole [8], the magnedial ring composed of the magnetic tune block will modulate the air gap's magnetic field formed by the high-speed rotor and the low-speed rotor so that the magnetic electrode logs different high-speed rotor, and the low-speed rotor form a magnetic field coupling and then transfers the rotational speed and torque.

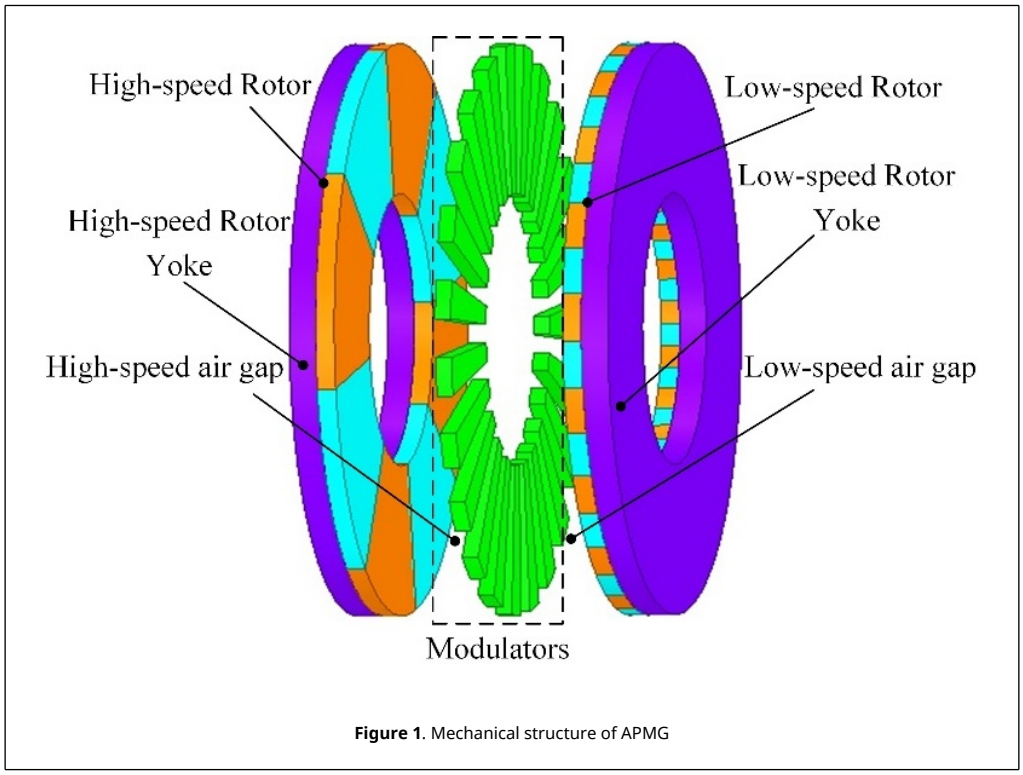

Figure 1. Mechanical structure of APMG

For convenient analysis, the air gap between the high-speed rotor and the magnetic tune ring in Figure 1 is called the high-speed side air gap, while the air gap between the magnetic tune ring and the low-speed rotor is called the low-speed side air gap.

As shown in Figure 1, the axial magnetic road of APMG is long, and the magnetic resistance of the magnetic flux line traveling from the high-speed rotor through the low-speed rotor is large, which makes it difficult to close the axial, radial and end magnetic road. This fact produces an increase of the leakage of magnetic and magnetic loss and a low utilization rate of the permanent magnet, transmitted torque and operation efficiency.

In order to reduce the leakage and magnetic loss of APMG, an additional modulation (hereinafter referred to as outer modulations) shown in Figure 2, is added to the outer side of the existing APMG low-speed rotor, while the former magnetic ring is still between the high-speed rotor and the low-speed rotor (hereinafter referred to as internal modulations).

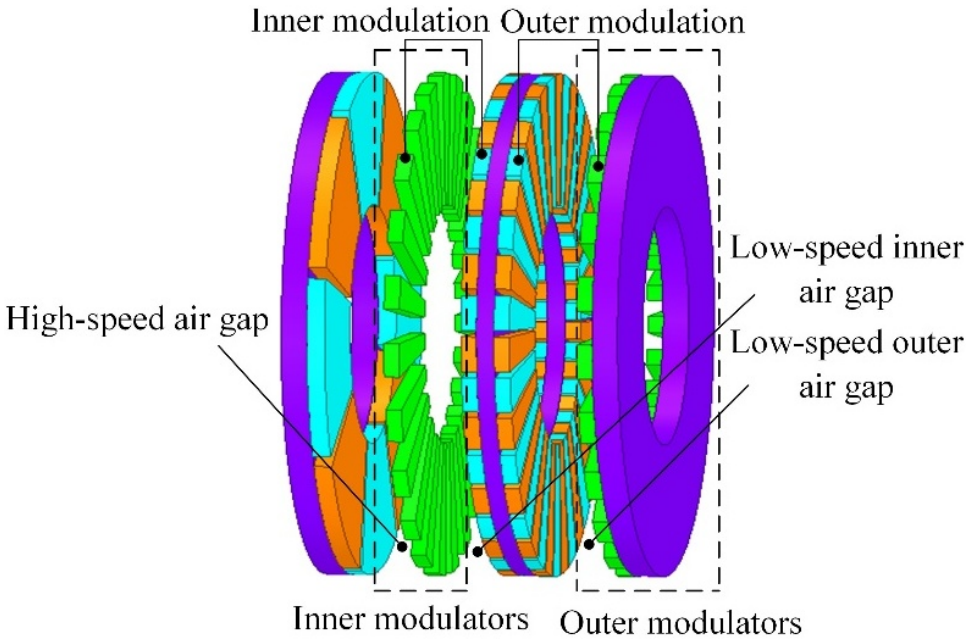

Figure 2. Mechanical structure of DEM-APMG

For convenient analysis, the air gap between the high-speed rotor and the internal regulating magnetic ring in Figure 2 is called the high-speed side; the air gap between the low-speed rotor and the internal regulating magnetic ring and is called the low-speed side internal air gap; and the air gap between the external regulating magnetic ring is called the low-speed side external air gap.

Figure 2 shows that the introduction of external magnetic ring causes the low-speed rotor to be clamped between the inner and outer magnetic rings, thus generating bidirectional excitation field. At the same time, the inner and outer magnetic rings modulate the low-speed rotor bidirectionally. It reduces the reluctance of inner and outer magnetizing ring modulated flux lines, makes more flux lines pass through the low-speed rotor, and improves the utilization ratio of the low-speed permanent magnet. In addition, the introduction of external magnetic ring also converts APMG axial leakage flux modulation into useful harmonics, which is applied to the low-speed rotor again. That is, after the introduction of the outer magnetic ring, the DEM-APMG structure formed by the outer magnetic ring can better solve the problems of high leakage, low torque density and low transmission efficiency of APMG.

3. DEM-APMG air gap magnetic field and electromagnetic torque model

Let the magnetic pole log of the DEM-APMG high-speed rotor and low-speed rotor be equal to p_h and p_l, respectively. The internal and external magnetic modulation blocks are the same, and the number of magnetic modulation blocks is equal to n_m and n_s, respectively.

To make the internal and external adjustable magnetic rings achieve the same modulation effect, the following equation should be met:

$$n_m = n_s = p_h + p_l \tag{1}$$

The internal and external magnetic rings are all stators. When the structure shown in Figure 2 is speed increasing, should be equal to the ratio of the high-speed rotor pole pairs to the low-speed rotor pole pairs, and the transmission ratio is:

$$G_{r1} = -\frac{p_l}{p_h} \tag{2}$$

In contrast, it is:

$$G_{r2} = -\frac{P_h}{P_l} \tag{3}$$

The negative sign of "-" in Eqs.(2) and (3) indicate the opposite direction of rotation of the two rotors.

When the spatial harmonic speed of the high- and low-speed permanent magnet rotor is the same, the DEM-APMG can transmit the rotational speed and torque stably; therefore,

$$\omega_l = G_{r2} \cdot \omega_h \tag{4}$$

where ω_l and ω_h are the angular velocities of the high-speed and low-speed rotors, respectively.

When the magnetic tune ring is not present, the axial and tangential components of the DEM-APMG high-speed side and low-speed side are, respectively:

$$B_{z1} = \sum_{i=1,3,5}^{+\infty} b_z^i(r,z,\theta) \cdot \cos\left[ip(\theta - \omega_1 t - \varphi_{z1,0})\right] \tag{5}$$

$$B_{\theta 1} = \sum_{i=1,3,5}^{+\infty} b_\theta^i(r,z,\theta) \cdot \sin\left[ip(\theta - \omega_1 t - \varphi_{\theta 1,0})\right] \tag{6}$$

In Eqs.(5) and (6), r, z and θ represent three variables, respectively, r represents the air gap magnetic density at different radii, z represents the air gap magnetic density at different axial lengths, and θ represents the air gap magnetic density at different tangential lengths, and where b_z^i and b_θ^i are the Fourier coefficient; i is harmonic number; p is magnetic pole logarithm of the permanent magnet; ω_1 is the rotation angular velocity of the permanent magnet, and $\varphi_{z1,0}$ and $\varphi_{\theta 1,0}$ are the axial and tangential initial phase angles of the permanent magnet rotor, respectively.

With the magnetic modulation ring, the air gap magnetic density changes at the high-speed side and at the low-speed side, and the axial and tangential air gap magnetic flux distribution functions are, respectively:

$$B_{z2} = b_{z2}^0(r,z,\theta) + \sum_{j=1,2,3}^{+\infty} b_{z2}^j(r,z,\theta) \cdot \cos\left[jn_m(\theta - \omega_m t - \varphi_{z2,0})\right] \tag{7}$$

$$B_{\theta 2} = b_{\theta 2}^0(r,z,\theta) + \sum_{j=1,2,3}^{+\infty} b_{\theta 2}^j(r,z,\theta) \cdot \sin\left[jn_m(\theta - \omega_m t - \varphi_{\theta 2,0})\right] \tag{8}$$

where b_{z2}^0, b_{z2}^j, $b_{\theta 2}^0$ and $b_{\theta 2}^j$ are the Fourier coefficients; ω_m is the rotation angular velocity of the magnetic ring; and $\varphi_{z2,0}$ and $\varphi_{\theta 2,0}$ are the axial and tangential initial phase angles of the flux modulated, respectively.

Because the numbers of internal and external modulation blocks are equal, the air gap flux distribution function is similar to Eqs.(7) and (8); thus, there are:

$$B_{z3} = b_{z3}^0(r,z,\theta) + \sum_{m=1,2,3}^{+\infty} b_{z3}^m(r,z,\theta) \cdot \cos\left[mn_s(\theta - \omega_s t - \varphi_{z3,0})\right] \tag{9}$$

$$B_{\theta 3} = b_{\theta 3}^{0}(r,z,\theta) + \sum_{m=1,2,3}^{+\infty} b_{\theta 3}^{m}(r,z,\theta) \cdot \sin\left[mn_s(\theta - \omega_s t - \varphi_{\theta 3,0})\right] \tag{10}$$

where b_{z3}^{0}, b_{z3}^{j}, $b_{\theta 3}^{0}$ and $b_{\theta 3}^{j}$ are Fourier coefficients; ω_s is the rotation angular velocity of the external tuning ring; $\varphi_{z3,0}$ and $\varphi_{\theta 3,0}$ are the axial and tangential initial phase angles of the flux of the external modulation block, respectively.

The axial component of the DEM-APMG air gap magnetic by multiplying Eqs.(5), (7) and (9) at different radii B_z:

$$\begin{aligned} B_z(r,z,\theta) &= B_{z1} \cdot B_{z2} \cdot B_{z3} \\ &= \sum_{i=1,3,5}^{+\infty} \sum_{j=1,2,3}^{+\infty} \sum_{m=1,2,3}^{+\infty} b_z^{0,i,j,m}(r,z,\theta) \\ &\cos\left[(ip + jn_m + mn_s)\left(\theta - \frac{ip\omega_r + jn_m\omega_m + mn_s\omega_s}{ip + jn_m + mn_s}\right) - (ip\varphi_{z1,0} + jn_m\varphi_{z2,0} + mn_s\varphi_{z3,0})\right] \end{aligned} \tag{11}$$

Multiplying Eqs. (6), (8) and (10) yields the tangential component of the DEM-APMG air gap at different radii B_θ:

$$\begin{aligned} B_\theta(r,z,\theta) &= B_{\theta 1} \cdot B_{\theta 2} \cdot B_{\theta 3} \\ &= \sum_{i=1,3,5}^{+\infty} \sum_{j=1,2,3}^{+\infty} \sum_{m=1,2,3}^{+\infty} b_z^{0,i,j,m}(r,z,\theta) \\ &\cos\left[(ip + jn_m + mn_s)\left(\theta - \frac{ip\omega_r + jn_m\omega_m + mn_s\omega_s}{ip + jn_m + mn_s}\right) - (ip\varphi_{z1,0} + jn_m\varphi_{z2,0} + mn_s\varphi_{z3,0})\right] \end{aligned} \tag{12}$$

Because Eqs.(11) and (12) are summed up along the DEM-APMG axial and tangential directions shown in Figure 2, respectively, the proposed model includes axial, tangential and end magnetic leakage, and the calculation accuracy should be consistent with the 3D finite element analysis.

Based on Eqs.(11) and (12) and using Maxwell stress tensor method, the DEM-APMG electromagnetic torque T_k can be obtained :

$$T_k = \frac{r_2^3 - r_1^3}{3\mu_0} \cdot \sum_{k=1,2,3}^{+\infty} B_z^k(r,z,\theta) B_\theta^k(r,z,\theta) \cos\left(\varphi^k{}_z - \varphi^k{}_\theta\right) \tag{13}$$

where r_2 and r_1 are the outer radius and the inner half meridian of the rotor, respectively, μ_0 is the vacuum magnetic conductivity, and k is the number of harmonics.

In Eq.(13), T_k is related to $B_z^k(r,z,\theta)$, $B_\theta^k(r,z,\theta)$ and $\cos\left(\varphi^k{}_z - \varphi^k{}_\theta\right)$; the electromagnetic torque T_k increases because the introduction of the external tuning magnetic ring can be effectively improved $B_z^k(r,z,\theta)$.

4. APMG and DEM-APMG performance comparison

Table 1 shows the required comparative APMG and DEM-APMG associated structural parameters. Comparison principle: the same inner and outer diameter and axial length of the APMG and DEM-APMG for each rotor.

Table 1. Initial values of the APMG and DEM-APMG structure

Symbol	Description	DEM-APMG	APMG
p_h	High-speed permanent magnet magnetic pole logarithmic	4	4
p_l	Low-speed permanent magnet magnetic pole logarithmic	19	19
n_m	Internal number of blocks	23	23
n_s	External number of blocks	23	
r_2	The outer radius of the rotor	105(mm)	105(mm)
r_1	The inner radius of the rotor	50(mm)	50(mm)
h_0	The air gap length of the magnetic loop	1(mm)	1(mm)
h_1	The rotor yoke iron axial length	10(mm)	10(mm)
h_2	The axial length of the high-speed permanent magnet	7(mm)	7(mm)

h_3	Axial length of internal tuning magnetic ring	6(mm)	6(mm)
h_4	The axial length of the low-speed permanent magnet	6(mm)	6(mm)
h_5	Axial length of external tuning magnetic ring	6(mm)	□
h_6	The axial length of the yoke of the external tuning magnetic ring	10(mm)	□
k	Magnetic block duty ratio	0.5	0.5
L	Total axial length	48(mm)	41(mm)

In Table 1, the permanent magnet material is NdFe35 and the magnetizing mode is axial. The yoke iron material is Q235. Based on the structural parameters shown in Table 1, the 3D finite element models of APMG and DEM-APMG are established and the static and dynamic simulation calculations are carried out to obtain the axial air gap magnetic density, torque capacity and axial force of the two structures.

4.1 Magnetic tight distribution of the air gap

The intermediate position of the high-speed side air gap of APMG and DEM-APMG and the air gap magnetic dense waveform scanned based on 3D finite element static simulation can describe the high-speed side and low-speed side shown in Figure 3. In Figure 3, the permanent magnet scanning radius is 50~105mm, the scan spacing is 1mm, and the scanning angle is 0~360°.

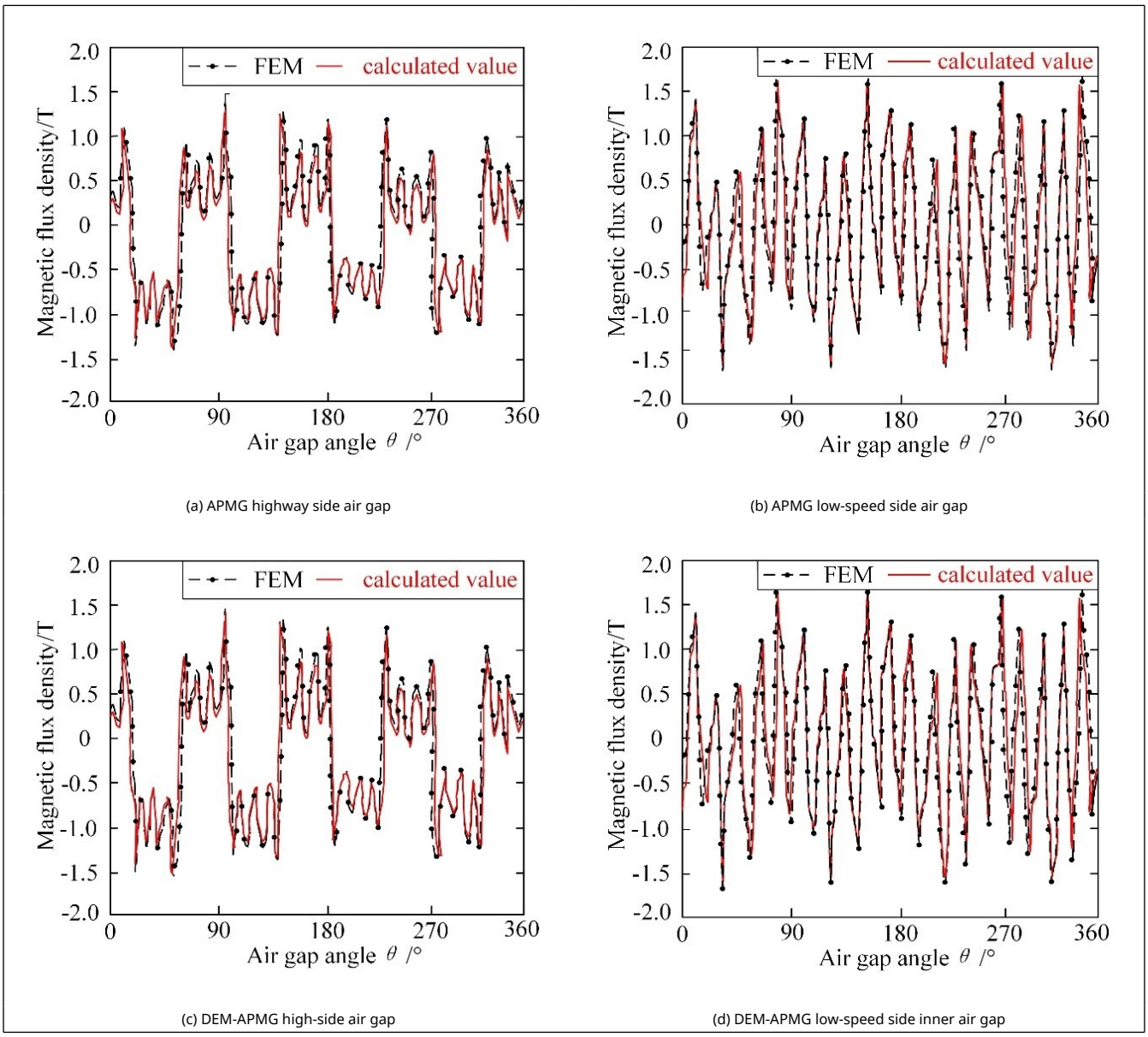

(a) APMG highway side air gap

(b) APMG low-speed side air gap

(c) DEM-APMG high-side air gap

(d) DEM-APMG low-speed side inner air gap

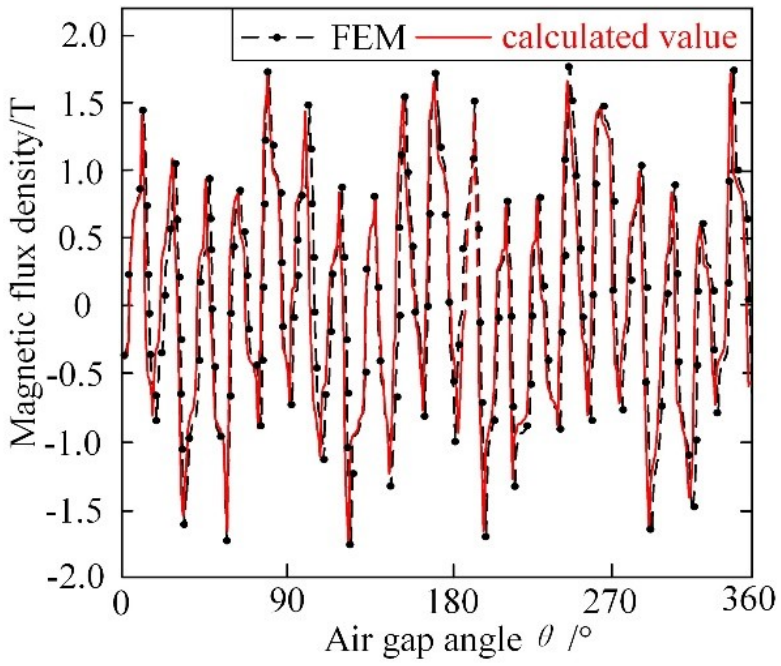

(e) DEM-APMG low-speed side outer air gap

Figure 3. Air-gap magnetic dense waveforms of the APMG and DEM-APMG

As shown in Figure 3(a) and Figure 3(c), there are 8 main waveforms and 38 harmonic shapes in the high-speed side air gap magnetic field, which are matched with the logarithms of the magnetic poles of the high-speed and low-speed rotors respectively. The air gap magnetic fields on the low-speed side shown in Figure 3(b), Figure 3(d) and Figure 3(e) are all 38 harmonic shapes, which are equal to the logarithm of the poles of the low-speed rotor. This shows that the inner and outer magnetic ring modulates the high-speed and low-speed rotors correctly and forms the required specific transmission speed and torque.

According to Figure 3, the air gap magnetic density on the APMG high-speed side and the low-speed side is 1.4~ -1.42T and 1.6~ -1.65T, respectively; that of the DEM-APMG is 1.47~ -1.53T, and that of the low-speed side is 1.6~ -1.65T and 1.75~ -1.75T, respectively. Therefore, the external magnetic ring can improve the air gap flux density of the DEM-APMG, transform the axial leakage flux modulation of the APMG into useful magnetic field harmonics, and improve the output torque and torque density.

The calculation time of 3D finite element is 1h, while the mathematical and physical model built in this paper is only 0.2h, and does not include the necessary time for model establishment, meshing and solution setup of 3D finite element. Therefore, the model built in this paper is not only accurate but also timesaving, and can quickly and accurately obtain DEM-APMG air gap magnetic density waveform and its numerical calculation results.

4.2 Torque capacity

4.2.1 Static torque capacity

The 3D static simulation model of the structural parameters shown in Table 1 was developed in the Ansys Maxwell environment, with the static torque simulation curves of the APMG and DEM-APMG rotor shown in Figure 4.

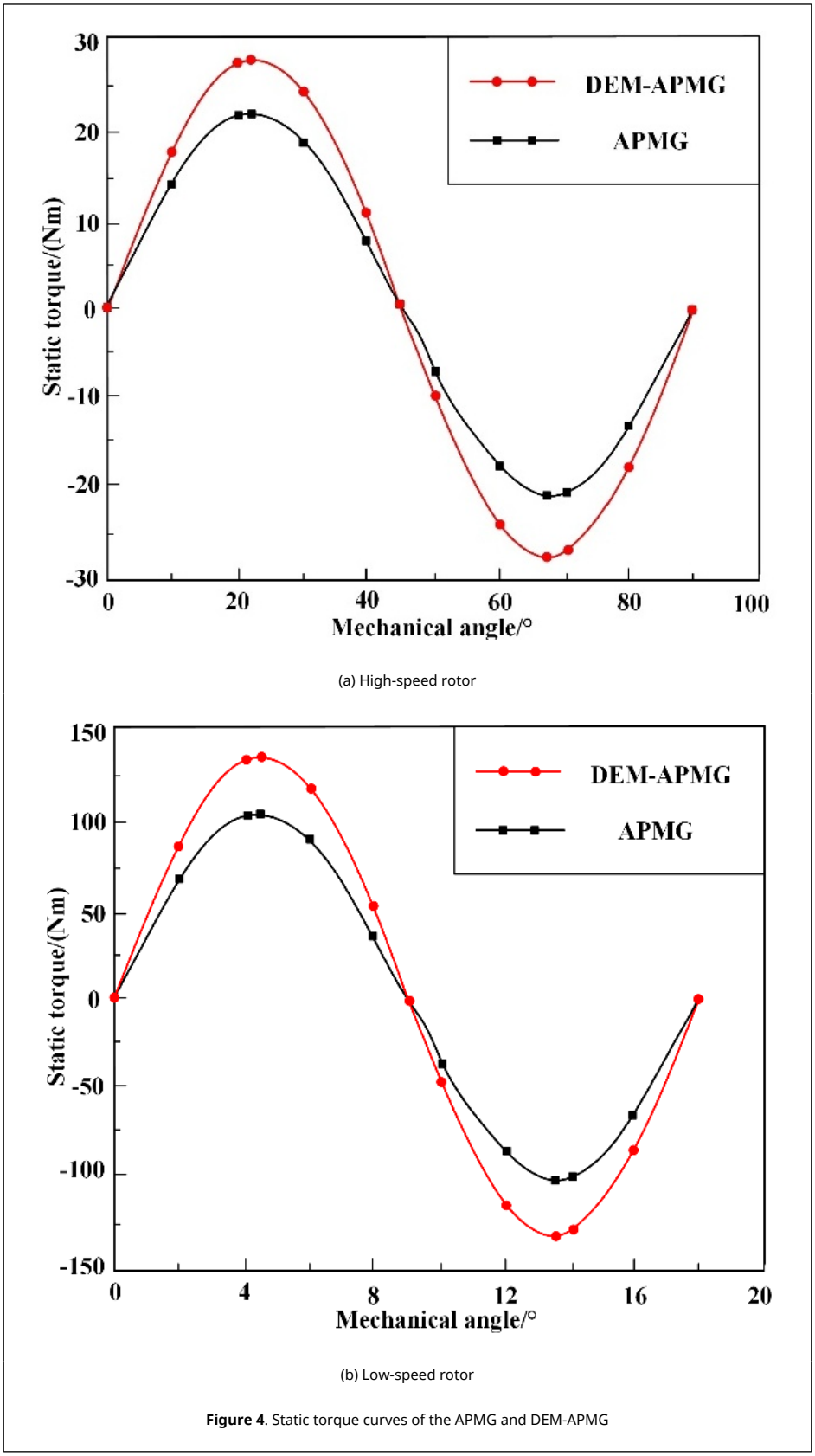

Figure 4. Static torque curves of the APMG and DEM-APMG

Figure 4(a) shows the static torque of a pair of permanent magnet rotor when the low-speed rotor moves motionless. Figure 44(b) shows the static torque of the rotation of a low-speed rotor with a high-speed rotor moves motionless.

As shown in Figures 4(a) and 4(b), the electromagnetic torque of both the high-speed and low-speed rotors are sinusoidal curves.

In Figures 4(a) and 4(b), the maximum static torque of the APMG high-speed and low-speed rotors is 22Nm and 105Nm, respectively; their ratio is near the set transmission ratio of 4.75, and the calculated torque density of the low-speed rotor is 108kNm/m^3. The maximum static torque of the DEM-APMG is 27.5Nm and 130Nm, respectively; the ratio is near the set transmission ratio of 4.75, and the calculated torque density of the low-speed rotor is 134kNm/m^3.

Based on this analysis, the maximum static torque of the DEM-APMG increased by 22.7% and 23.8% compared with that of the APMG, respectively, and the torque density increased by 24%.

In addition, as the calculation time of air-gap magnetic density is the same, the finite element calculation time of Figures 4(a) and 4(b) is 1h, while the theoretical calculation time of the mathematical and physical model built in this paper is 0.2h. It also shows that the torque model built in this paper is not only accurate, but also time-consuming, and the DEM-AFMPMG electromagnetic torque waveform and its numerical results can be quickly and accurately obtained.

4.2.2 Dynamic torque capacity

Similarly, the 3D dynamic simulation model of the structural parameters shown in Table 1was developed in the Ansys Maxwell environment, where the input speed of the high-speed rotor was 1500rpm, and the output speed of the low-speed rotor was -1500/4.75=-315.8rpm (the negative number indicates the opposite direction of rotation of the high-speed rotor and the low-speed rotor) to determine the steady-state torque simulation curve of the APMG and DEM-APMG shown in Figure 5.

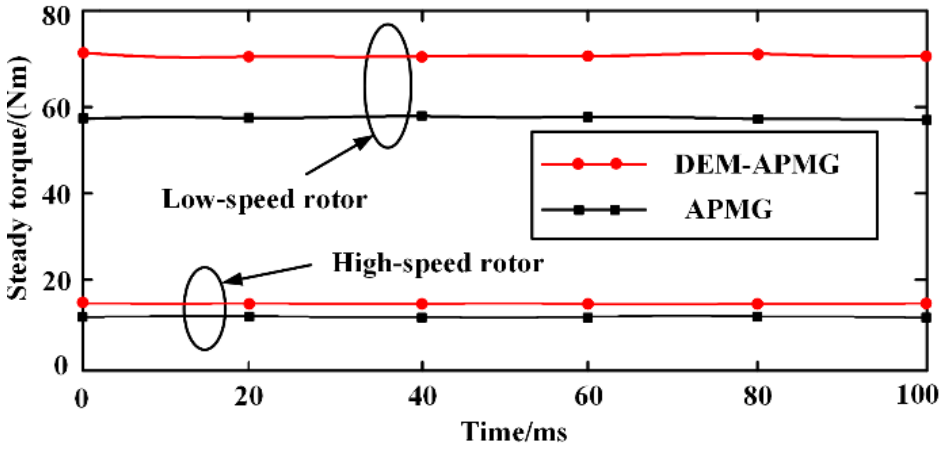

Figure 5. APMG and DEM-APMG steady-state torque curves

From Figure 5, the steady state torque of the high-speed and low-speed rotor of APMG are 11.9Nm and 56Nm, respectively; those of the high-speed and low-speed rotor of DEM-APMG are 15Nm and 72Nm, respectively. Therefore, the output torque of the DEM-APMG rotor of the same size at steady-state operation increased by 26% and 29% compared with the APMG, respectively.

4.3 Steady-state axial magnetic pull

The input speed of the high-speed rotor is fist set to 1500rpm. Then, the output speed of the low-speed rotor is -315.8rpm. After the 3D finite element simulation, the steady-state axial magnetic pull of the APMG and DEM-APMG is shown in Figure 6.

Figure 6 shows that the axial magnetic tensions of the high-speed and low-speed rotors of the APMG are 5.2kN and -9kN, respectively, and those of the DEM-APMG are 3.8kN and -0.8kN, respectively. The axial magnetic tensile force of the magnetodial ring is 14.2kN, and the internal and external dial rings of the DEM-APMG are 4.6kN and 0.8kN, respectively. Thus, the axial magnetic tensile force in the DEM-APMG decreased by 68% and 94% compared with the APMG, respectively.

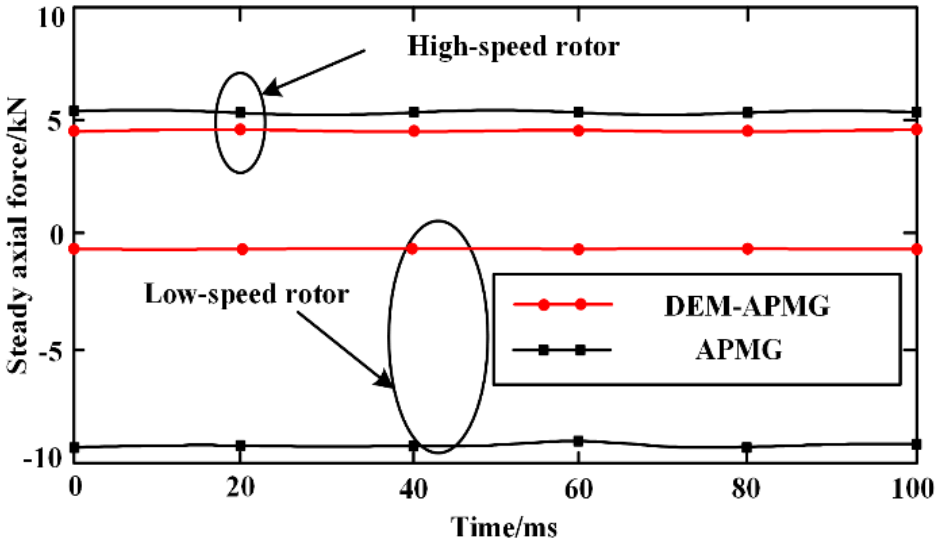

Figure 6. APMG and DEM-APMG steady-state axial magnetic pull

5. Effects of the major structural parameters on the torque density

Torque density is an important measure of permanent magnet gear transmission performance [9]. The influence of the primary structural parameters on the DEM-APMG torque density when the axial length of the rotor yoke and $G_r = -4.75$ is held constant.

5.1 Influence on the torque density for h_2 and $h_4$5.1 Influence on the torque density for h 2 {\textstyle {\it {h}} {2}} and h 4 {\textstyle {\it {h}} {4}}

When fixed h_4 and other structural parameters remain unchanged, the influence curve on torque density shown in Figure 7 can be obtained only when h_2 is from 5 to 15mm.

Similarly, the influence curve on torque density shown in Figure 8 can be obtained only when h_4 is from 5 to 15mm , fixed h_2 and other structural parameters remain unchanged.

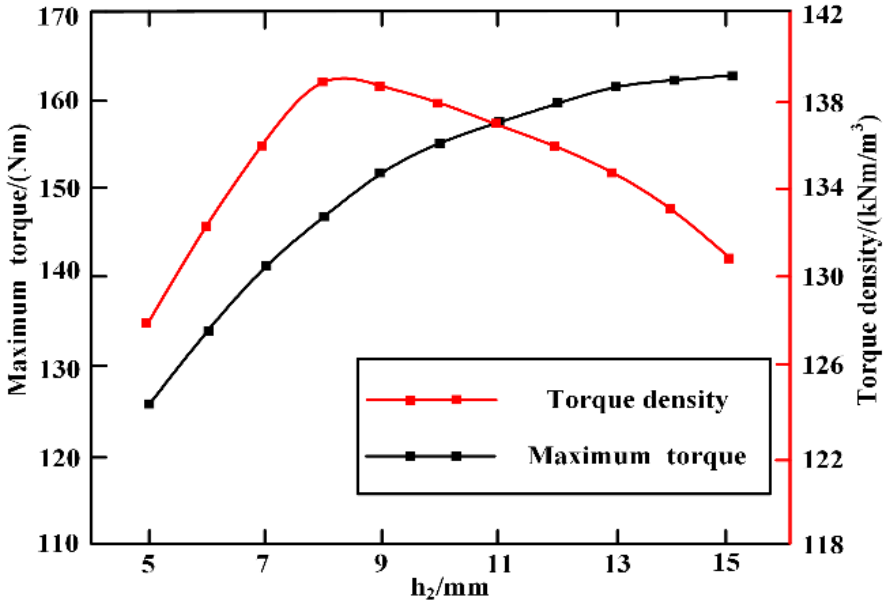

Figure 7. Effect curve of the axial length of high-speed permanent magnets on the torque density

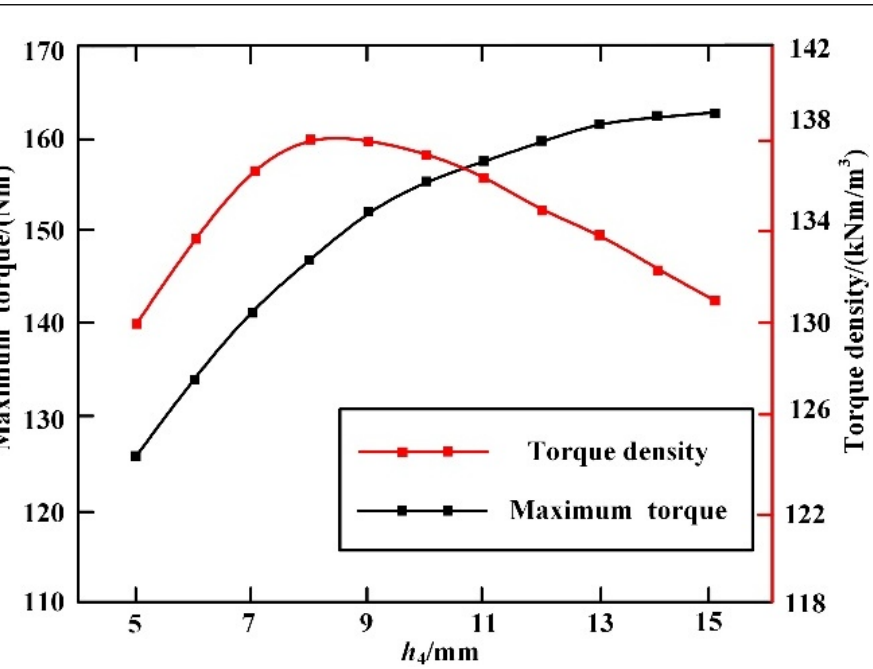

Figure 8. Effect curve of the axial length of the low-velocity permanent magnet on the torque density

Figure 8 shows that the maximum output torque increases as h_2 increases. However, when $h \geq 13.5$ mm, the rate of increase of the maximum output torque slows; at $h_2 = 8$ mm, the torque density peaks at 139kNm/m^3 and then gradually decreases as h_2 increases. This result occurs because the DEM-APMG air gap flux density gradually reaches saturation, and then, the air gap flux density no longer increases, slowing the maximum output torque growth and then reducing the torque density.

The curve shown in Figure 8 is similar to Figure 7, and the maximum output torque increase slows down at $h_4 \geq 13.5$ mm. At $h_4 = 13.5$ mm, the torque density peaks at 139kNm/m^3.Thus, the torque density of DEM-APMG is maximized at

h_2 = h_4 = 8 mm.

5.2 Influence on the torque density for r_1 and $r_2$5.2 Influence on the torque density for r 1 {\textstyle {\it {r}} {1}} and r 2 {\textstyle {\it {r}} {2}}

When fixed r_2 and other structural parameters remain unchanged, the influence curve on torque density shown in Figure 9 can be obtained only when r_1 is from 40 to 90mm.

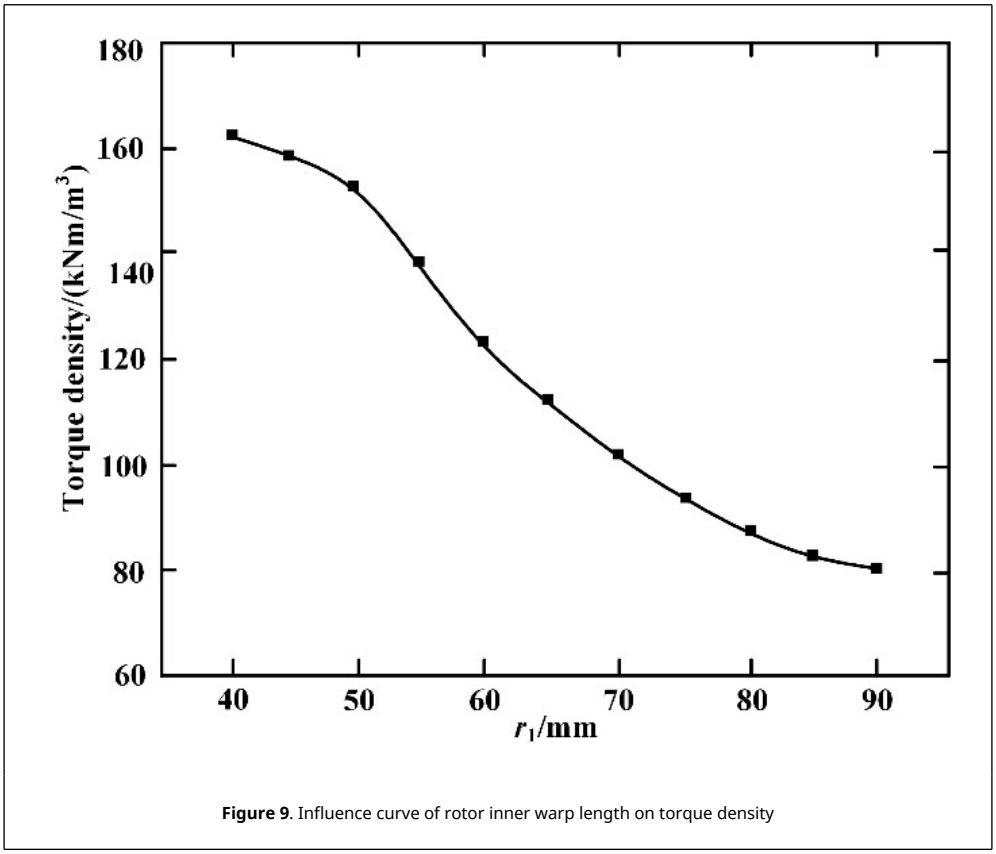

Figure 9. Influence curve of rotor inner warp length on torque density

As shown in Figure 9, the torque density decreases with increasing r_1. This result occurs because the increase in r_1 leads to a decrease in the permanent magnet consumption, the DEM-APMG magnetic energy product decreases, and the output torque and torque density decrease. The torque density decreases linearly when r_1 < 50 mm and in a hyperbolic form when r_1 > 50 mm.

In Figure 9, the torque density is 155kNm/m^3 when r_1 = 50 mm. At r_1 = 40 mm, the torque density is 165kNm/m^3. Therefore, the torque density of mm is only 6% compared with r_1 = 50 mm, and r_1 = 40 mm occurs at the linear and hyperbolic critical point shown in Figure 9 at r_1 = 50 mm; thus, r_1 = 50 mm is the best value.

5.3 Influence on the torque density for h_3 and $h_5$5.3 Influence on the torque density for h 3 {\textstyle {\it {h}} {3}} and h 5 {\textstyle {\it {h}} {5}}

When fixed h_5 and other structural parameters remain unchanged, the influence curve on torque density shown in Figure 10 can be obtained only when h_3 is from 3 to 13mm.

Similarly, the influence curve on torque density shown in Figure 11 can be obtained only when h_5 is from 3 to 13mm , fixed h_3 and other structural parameters remain unchanged.

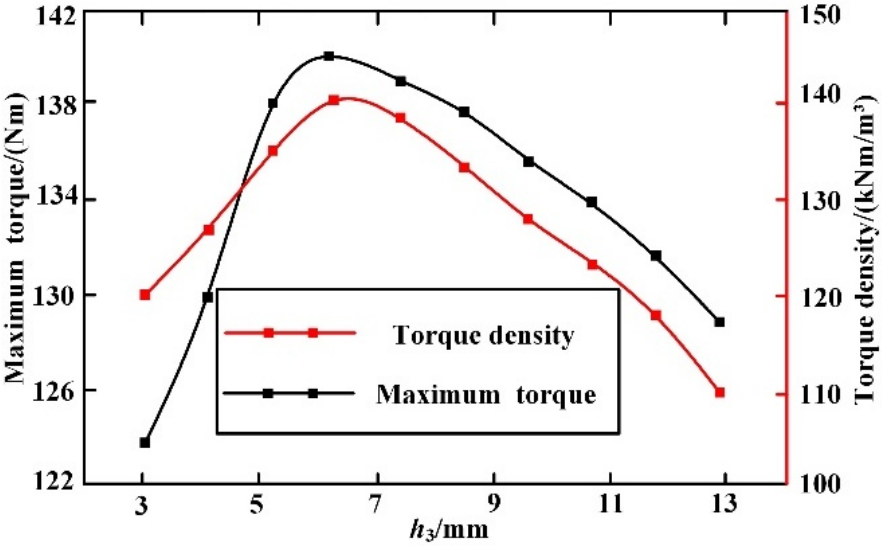

Figure 10. Influence curve of axial length of internal magnetic block on torque density

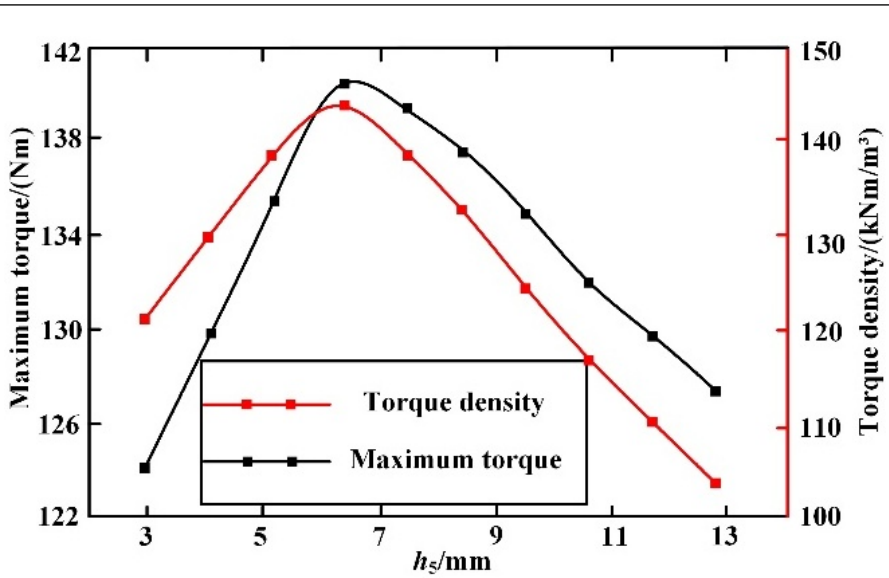

Figure 11. Influence curve of axial length of external magnetic block on torque density

As shown in Figure 10, the maximum output torque and torque density change similarly. When the torque density increases from 3mm to 6mm, the torque density and maximum output torque gradually increase. At h_3 = 6 mm, the torque density and maximum output torque peak at 140Nm and 140kNm/m^3, respectively. Thus, both the torque density and the maximum output torque gradually decrease because h_3 >at the hour, the internal gap loop is magnetized, but the air gap magnetic field of the permanent magnet is not. Also, the air gap magnetic path is longer, and the magnetic resistance and leakage increase, decreasing the torque density and maximum torque.

The curve shown in Figure 11 is similar to that in Figure 10, and when h_5 = 6 mm, the maximum output torque and torque density peak are 141Nm and 141kNm/m^3, respectively, and will also gradually decrease later.

Thus, the torque density of DEM-APMG is maximized when h_3 = h_5 = 6 mm.

5.4 Influence on the torque density for k5.4 Influence on the torque density for k {\textstyle k}

The block duty cycle represents the ratio of the block volume to the entire tuning region [10]. When the other structural parameters remain unchanged, and only k is changed, we can determine the influence of k on the torque density, as shown in Figure 12, where k changes from 0.1 to 0.77.

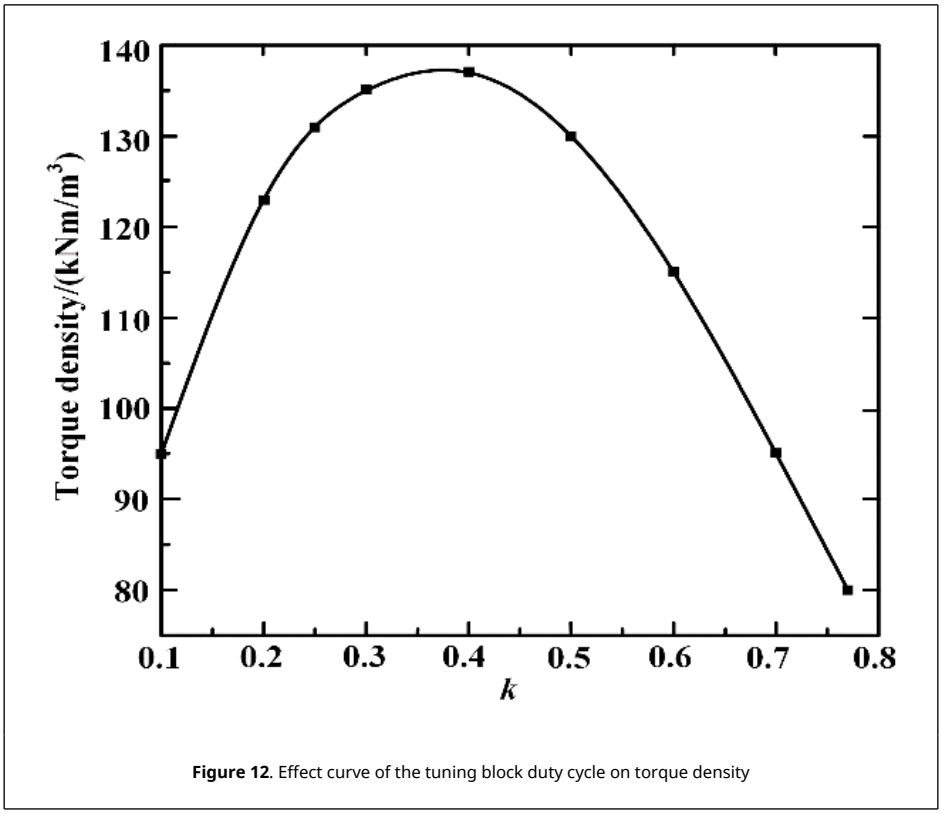

Figure 12. Effect curve of the tuning block duty cycle on torque density

As shown in Figure 12, the torque density increases when k < 0.4. When k = 0.4, the peak torque density is reached (138kNm/m^3), which will then gradually decrease as k increases.

Therefore, at k = 0.4, the torque density of DEM-APMG is maximized.

Thus, the optimal parameters are shown in Table 2 and the other unmodified parameters are shown in Table 1.

Table 2. Optimal structural parameters for the DEM-APMG

Symbol	Description	Numerical (unit)
h_2'	The axial length of the high-speed permanent magnet	8(mm)
h_4'	The axial length of the low-speed permanent magnet	8(mm)
k	Magnetic block duty ratio	0.4

Based on the structural parameters shown in Tables 1 and 2, the optimized 3D DEM-APMG in the Ansoft environment has a torque density of 156kNm/m^3, which is an approximately 16% improvement over the preoptimized DEM-APMG.

6. Conclusions

(1) An APMG is composed of a high-speed rotor, a low-speed rotor and a magnetic modulation ring. Although the mechanical structure is simple, its axial magnetic resistance and leakage magnetic flux are both large, resulting in a low utilization rate of the permanent magnet and a low maximum output torque and torque density.

(2) The DEM-APMG introduces an external magnetic ring based on the APMG structure, which causes the internal and external magnetic rings to exhibit bidirectional excitation and bidirectional modulation to reduce the axial magnetic resistance and axial magnetic leakage of the low-speed rotor. This structure also converts the APMG into useful

harmonics and also on the low-speed rotor, thus increasing the output torque and torque density of the DEM-APMG.

(3) The maximum static torque of DEM-APMG at the same external diameter increased by 22.7% and 23.8% compared with APMG and 26% and 29% at steady-state operation, while the torque density increased by 24%.

(4) 3D finite element analysis shows that the structural parameters with the greatest impact on DEM-APMG torque density are the axial length of the block duty cycle and high-speed and low-speed permanent magnets. When the axial length of the high-speed and low-speed permanent magnets is 8mm and the duty cycle is 0.4, the DEM-APMG torque density reaches 156kNm/m^3.

References

[1] Atallah K., Howe D. A novel high-performance magnetic gear. IEEE Transactions on Magnetics, 37(4):2844-2844, 2001.

[2] Mezani S., Atallah K., Howe D. A high-performance axial-field magnetic gear. Journal of Applied Physics, 99(8):83-88, 2006.

[3] Gardner M.C., Jack B.E., Johnson M., Toliyat H.A. Comparison of surface mounted permanent magnet coaxial radial flux magnetic gears independently optimized for volume, cost, and mass. IEEE Transactions on Industry Applications, 54(3):2237-2245, 2018.

[4] Johnson M., Shapoury A., Boghrat P., Post M., Toliyat H.A. Analysis and development of an axial flux magnetic gear. 2014 IEEE Energy Conversion Congress and Exposition (ECCE), 5893-5900, 2014.

[5] Tsai M.C., Ku L.H. 3D printing-based design of axial flux magnetic gear for high torque density. IEEE Transactions on Magnetics, 51(11):1-4, 2015.

[6] Afsari Kashani S.A. Optimal design and analysis of a novel reluctance axial flux magnetic gear. Scientia Iranica, 29(3):1573-1580, 2022.

[7] Ge Y.J., Nie C.Y., Xin Q. A three dimensional analytical calculation of the air-gap magnetic field and torque of coaxial magnetic gears. Progress in Electromagnetics Research, 131:391-407, 2012.

[8] Sepaseh J., Rostami N., Feyzi M.R. An axial magnetic gear with improved torque density and reduced cogging torque. Iranian Journal of Electrical and Electronic Engineering, 17(4):2043-2043, 2021.

[9] Darabi A., Abolghasemi M., Mirzahosseini R., Sarvi-Maraghi M. Transient analysis of an axial flux magnetic gear. 2020 28th Iranian Conference on Electrical Engineering (ICEE), 1-5, 2020.

[10] Kouhshahi M.B, Acharya V.M., Calvin M., Bird J.Z., Williams W. Designing and experimentally testing a flux-focusing axial flux magnetic gear for an ocean generator application. IET Electric Power Applications, 13(8):1212-1218, 2019.